# A Highly Hydroxide Conductive, Chemically Stable Anion Exchange Membrane, Poly(2,6 dimethyl 1,4 phenylene oxide)-*b*-Poly(vinyl benzyl trimethyl ammonium), for Electrochemical Applications

**Tara P. Pandey,[a,=,*] Himanshu N. Sarode,[a,=,*] Yating Yang,[b] Yuan Yang,[b] Keti Vezzù,[c] Vito Di Noto,[c,**] Soenke Seifert,[d] Daniel M. Knauss,[b] Matthew W. Liberatore,[e] and Andrew M. Herring[a,**,z]**

[a]*Department of Chemical and Biological Engineering, Colorado School of Mines, Golden, Colorado 80401, USA*
[b]*Department of Chemistry and Geochemistry, Colorado School of Mines, Golden, Colorado 80401, USA*
[c]*X-Ray Sciences Division, Advanced Photon Source, Argonne National Laboratory, Argonne, Illinois 60439, USA*
[d]*Department of Industrial Engineering, Section of Chemistry for Technology and Energy and Department of Chemical Sciences, University of Padova, I-35131 Padova, Italy*
[e]*Department of Chemical and Environmental Engineering, University of Toledo, Toledo, Ohio 43606, USA*

A chemically stable copolymer [poly(2,6 dimethyl 1,4 phenylene oxide)-*b*-poly(vinyl benzyl trimethyl ammonium)] with two ion exchange capacities, 3.2 and 2.9 meq $g^{-1}$, was prepared as anion exchange membranes (AEM-3.2 and AEM-2.9). These materials showed high $OH^-$ conductivities of 138 $mS.cm^{-1}$ and 106 $mS.cm^{-1}$, for AEM-3.2 and AEM-2.9 respectively, at 60°C, and 95% RH. The $OH^-$ conductivity = 45 $mS.cm^{-1}$ for AEM-3.2 at 60% RH and 60°C in the absence of $CO_2$. Amongst the ions studied, only $OH^-$ is fully dissociated at high RH. The lower $E_a$ = 10–13 $kJ.mol^{-1}$ for $OH^-$ compared to $F^- \sim 20$ $kJ.mol^{-1}$ in conductivity measurements, and of $H_2O$ from self-diffusion coefficients suggests the presence of a Grotthuss hopping transport mechanism in $OH^-$ transport. PGSE-NMR of $H_2O$ and $F^-$ show that the membranes have low tortuosity, 1.8 and 1.2, and high water self-diffusion coefficients, 0.66 and 0.26 × $10^{-5}$ $cm^2.s^{-1}$, for AEM-3.2 and AEM-2.9 respectively. SAXS and TEM show that the membrane has several different sized water environments, ca. 62 nm, 20 nm, and 3.5 nm. The low water uptake, λ = 9–12, reduced swelling, and high $OH^-$ conductivity, with no chemical degradation over two weeks, suggests that the membrane is a strong candidate for electrochemical applications.


Manuscript submitted February 24, 2016; revised manuscript received March 31, 2016. Published April 9, 2016.

Anion Exchange membranes (AEMs) have been proposed as the separator in electrochemical energy conversion devices such as fuel cells, electrolyzers, or redox flow cells.[1] As catalysis is more facile in base, the use of an AEM should allow the use of non-precious metal catalysts and also the oxidation or production of complex fuels beyond hydrogen.[2] Significant work has been done in the past decade in this area and many new membranes have been developed with improved mechanical, chemical, and transport properties. An ideal AEM should have high ionic conductivity to achieve practical power densities,[3] good chemical stability to operate under an alkaline environment,[4] and excellent thermal and mechanical properties to survive transient operating conditions.[1,5] Intensive efforts have been made to study AEMs with aromatic backbones such as polysulfone,[6–8] poly(2,6-dimethyl-1,4-phenylene oxide) (PPO),[9–11] and poly(ether ether ketone)[12] due to their high thermal and chemical stability, good mechanical properties, and outstanding film forming ability.[13] PPO is a versatile aromatic polymer, which can advantageously be used as a precursor in the preparation of graft,[14] random and copolymers as studied by previous researchers for AEM applications.[9,11,15,16] PPO was found to be favorable in the fabrication of AEMs due to its higher alkaline stability stemming from the absence of strong electron-withdrawing groups. The polymer has been studied using solvent processing techniques earlier[17] but no study reports melt processing for fabricating membranes.

Polymer – water/ion interactions are important when it comes to understanding performance of anion exchange membranes.[18] Inherently hydroxide ($OH^-$) transport (5.273 × $10^{-5}$ $cm^2$/sec) is ∼50% slower than proton transport (9.30 × $10^{-5}$ $cm^2$/sec) in free water which potentially could decrease the performance of AEMFCs compared to membranes of the same thickness as in PEMFCs.[19] $OH^-$ conductivities are often lower than corresponding proton conductivities at hydrated conditions and reduce drastically under relatively drier conditions of operation. Ionic conductivity can be improved by higher ionic content with addition of more ion conducting groups. However, this method tends to result in excessive water uptake and swelling, therefore, compromising the mechanical properties of the membrane. Hydration is equally important for creating water filled continuous channels, which facilitate $OH^-$ transport by Grotthuss hopping, which has been reported to be faster than just diffusive transport. In water both proton and $OH^-$ ions are transported by structural diffusion (Grotthuss hopping) in addition to the vehicular process.[20–22] In order to overcome the drawbacks described above, the design and synthesis of new membranes need to be addressed by a complete understanding of the interplay that exists between structure, properties, ion migration mechanisms.[23] Phase separation was proven to increase ionic conductivity for AEMs while keeping low water uptake in a study of intensifying the cationic groups by installing multi-cationic groups on each pendent chain,[24,25] or extending the ionic repeat units by preparing block copolymer and graft copolymers,[26–28] or including long spacer chains in the quaternary ammonium cation.[29] Most of the previously reported chemistries concentrate on functionalizing PPO by bromination, but in this study we have kept PPO as a hydrophobic block and functionalized the polyvinylbenzylchloride (PVBC) block for $OH^-$ ion conduction.

Although it is common to report $OH^-$ conductivity for AEMs in liquid water, there are very few reports in the literature of the study of $OH^-$ and water transport in an AEM, under the conditions of humidification that are important to practical operation. This enables the properties to be reported as a function of λ (the number of waters per charge carrier). This is because of the nucleophilic nature of $OH^-$ and its propensity to chemically attack AEMs under hotter and drier conditions, as well as the rapid conversion of $OH^-$ to $CO_3^{2-}$ and $HCO_3^-$ in the presence of the ambient 400 ppm $CO_2$.[30] This research work reports a successful measurement of pure $OH^-$ ionic conductivity under humidified conditions and relates it to the air exposed

=These authors contributed equally in this work.
*Electrochemical Society Student Member.
**Electrochemical Society Member.
zE-mail: aherring@mines.edu

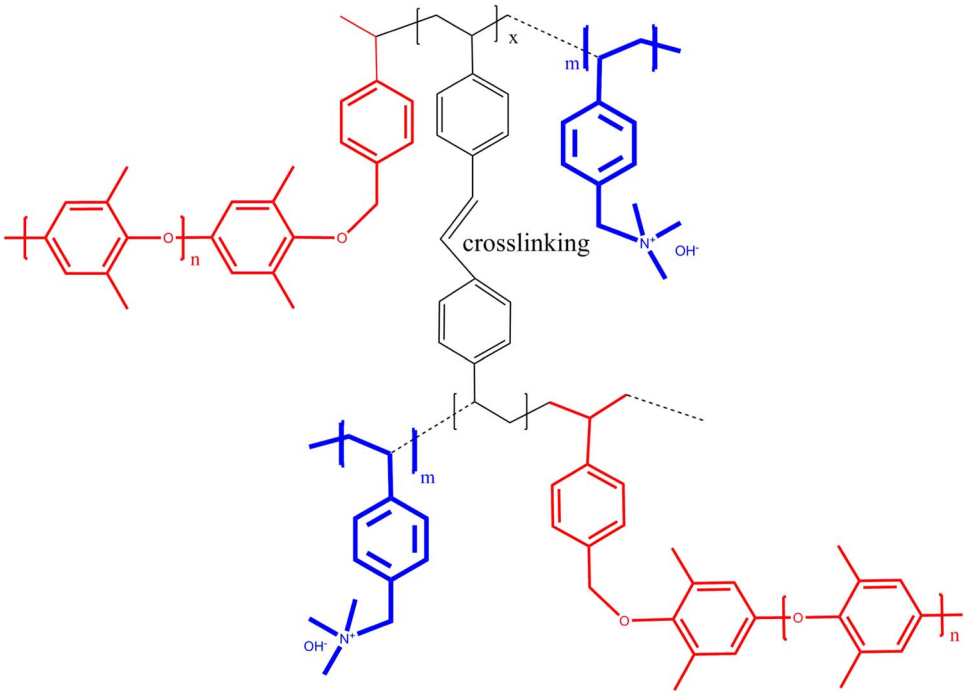


**Figure 1.** Chemical structure of cross-linked PPO-*b*-PVBTMA [$OH^-$] copolymer, the black color (thin bonds) represents thermally cross-linked PVBC, the red color (thick bonds) indicates the PPO backbone and the blue color (thickest bonds) represents the PVBTMA cation in the diblock copolymer structure.

$OH^-$ form of the membrane. Many other researchers report $OH^-$ conductivity[31] but very few researchers have successfully excluded residual $CO_2$ from their measurements.[32] The challenge to control the rapid reaction of $OH^-$ with $CO_2$, which changes the counter-anions to $HCO_3^-/CO_3^{2-}$ reducing ionic conductivity in the membrane, was realized in our previous work.[32,33] We reported the pure $OH^-$ form conductivity and studied the chemical stability of the AEM during this measurement. Structural understanding about the membrane has been obtained from pulse gradient stimulated spin echo (PGSE) NMR and small angle X-ray scattering (SAXS) experiments. Self-diffusion coefficients and in-plane ionic conductivity of $OH^-$ provides an idea of the ionic pathway and the types of ionic transport mechanisms in the membrane. Here, we report $OH^-$ conductivity and stability in a novel poly(2,6 dimethyl 1,4 phenylene oxide)-*b*-poly(vinyl benzyl trimethyl ammonium) (PPO-*b*-PVBTMA) based AEM[34] and the detailed study of transport in AEMs of this material with IECs of 3.2 and 2.9 meq $g^{-1}$ designated as AEM-3.2 and AEM-2.9; respectively.

## Experimental

Unless otherwise stated, all experimental measurements were performed under humidified conditions as a function of temperature. The '$OH^-$' represents hydroxide ions under controlled $N_2$ environment that excludes $CO_2$. The "air exposed $OH^-$" represents the membrane, which was exposed to ambient air for 24 h prior to performing experiments.

***Membrane preparation by melt pressing.—***The PPO-*b*-PVBC diblock copolymer powder was used as a base material for membrane preparation (chemical structure shown in Figure 1) which was synthesized as described earlier at the Colorado School of Mines.[34] A solvent cast membrane from chloroform ($CHCl_3$) was very brittle when dry and became gel-like when wet. Melt pressing of the diblock copolymer however, induced thermal cross-linking of hydrophilic block that resulted in an increased mechanical stability of the membrane. The melt pressing technique was similar to the published procedure.[34] The melt pressing of copolymer introduced cross-linking by dehydrochlorination[35] as shown in Figure 1. The melt pressed membrane was then soaked in 25wt% trimethyl amine solution for 24 h for the quaternization reaction to occur. The semi-transparent quaternary ammonium membrane in chloride form ($Cl^-$) was ion exchanged to bicarbonate ($HCO_3^-$), and $OH^-$ using methods previously published[32] for further studies.

***Ion exchange procedure.—***To exchange the membrane into the $HCO_3^-$ form, the $Cl^-$ form of the membrane was soaked in 1 M $NaHCO_3$ for 24 h, rinsed with DI water and vacuum dried at room temperature for 12 h. To exchange the membrane into the $OH^-$ form $CO_2$ free glove box was used.[32,36] The membrane was soaked in 1M KOH solution for 24 h, rinsed with Argon degassed DI water until neutral pH and ambient dried in the glove-box under $N_2$ environment. The membrane was loaded and sealed in a conductivity cell and transferred to experimental setup in $N_2$ environment for conductivity measurements. Membranes were exchanged to bromide form by exchanging in 1M KBr for 24 h followed by washing with DI water.

Conversion to the fluoride form of the membrane was achieved by soaking the membrane in ~3.5 M benzyl trimethyl ammonium fluoride solution for 3 days at room temperature and 500 psig $N_2$ pressure in a pressurized reactor (Parr Instruments, high pressure compact reactor) to achieve high ion exchange for NMR diffusion experiments.

***Conductivity measurements.—***The in-plane ionic conductivity was measured using a 4 probe custom built cell with 4 platinum electrodes. The measurement was carried out using a VMP3 potentiostat (Bio-Logic) running electrochemical impedance spectroscopy (EIS). Frequency was swept between 0.5 MHz to 0.3 Hz for the EIS experiment as a function of temperature, humidity and counterion. The humidity of each sample was controlled by using a Test Equity environmental chamber (Test Equity 1007H). For hydroxide conductivity measurements, it is important to exclude atmospheric $CO_2$ and thus equilibration for hydroxide conductivity samples was done in a modified BekkTech cell. For this measurement, a BekkTech fuel cell testing stand was modified to incorporate the 4 probe conductivity cell. The wet gas was produced by passing dry UHP $N_2$ gas through a heated humidity bottle from Fuel cell technologies. Humidity in

the sealed cell was controlled by supplying a mixture of dry and wet gas which was controlled by 2 mass flow controllers (1000SCCM, MKS, Andover, MA) and heated gas lines. Humidity was measured by a humidity probe (Vaisala HMT 337, Boulder, CO) fitted inside of the custom built oven. Oven, gas transfer lines, humidity bottle were all temperature controlled by external heaters. All temperature and humidity setpoints were controlled by the LabView software with homebuilt feedback control system. A detailed experimental setup of the modified BekkTech setup can be found here.[37]

The collected impedance spectra were fitted to the Randall circuit to find the total resistance of the membrane. The conductivity ($mS.cm^{-1}$) was calculated from the measured membrane resistance from: $\sigma = l/Rwt$ where $l$ is the distance between two electrodes ($l$ = 4.25 mm), $R$ is the resistance ($\Omega$); $w$ and $t$ are the width and thickness of the membrane.

***Ion exchange capacity (IEC) measurements.—***The ion exchange capacity of the diblock polymer before melt pressing was determined using NMR. The amount of PVBC group represented by NMR spectra in the polymer provided information about the IEC of starting polymer material before melt pressing.[34] A standard back-titration method, similar to the procedure in literature, was used to determine the IEC of the membrane after melt pressing and quaternization.[34,38]

***Water uptake and dimensional swelling measurements.—***A dynamic vapor sorption instrument (Surface Measurement System DVS Advantage 1) was used to measure the water vapor uptake in the $Cl^-$ form of the membrane. The membranes were vacuum dried at 30°C for 12 h prior to the experiment and transferred to the DVS instrument for the gravimetric measurement. The mass change was measured at humidity set points (0, 20, 40, 60, 80, and 95%RH), including 3 h drying step to get the initial mass at 0%RH at 60°C. Water uptake (WU) was calculated using the following equation.

$$\text{Water Uptake (WU)} = \frac{m_{\%RH} - m_{dry}}{m_{dry}}$$

where $m_{\%RH}$ and $m_{dry}$ represent the mass of the membrane samples at the given humidity and dry state; respectively. With the water uptake values at given relative humidity, IEC of the AEM and molecular weight of water, the hydration level ($\lambda$), which is the number of water molecules per cationic functional group can be calculated using following equation:

$$\lambda = \frac{n(H_2O)}{n(NR_4^+)} = \frac{WU \times 1000}{m(H_2O) \times IEC}$$

For liquid water uptake measurements, the vacuum dried membranes were weighed for dry measurements and then soaked in liquid water at room temperature for 24 h for taking the soaked weight measurements. The difference in the wet and dry weight of the membranes was used to calculate the liquid water uptake by the membranes. The membrane samples soaked in liquid water at room temperature for 24 h were taken out from water and quickly blotted using Kimwipes for removing any excess surface water. The thickness was measured with a digital micrometer and the in-plane dimension with a digital Vernier caliper to obtain wet membrane dimension. The membrane samples were then dried in a vacuum oven at 30°C for 24 h for thickness and in-plane measurements in the dry state and $OH^-$ water uptake in liquid water was measured in a glove box to exclude $CO_2$.The dimensional swelling of the membrane was calculated using the following equation:

$$\text{Dimensional swelling (\%)} = \frac{Dim_{wet} - Dim_{dry}}{Dim_{dry}} \times 100$$

where $Dim_{wet}$, and $Dim_{dry}$ represent the dimensions of the sample under wet and dry conditions; respectively.

***$H_2O$ and $F^-$ diffusion measurement using PGSE diffusion NMR.—***A 5 mm NMR tube was prepared by having two water reservoirs one below and one above the membrane sample (Figure S1) as opposed to having just one water reservoir below the membrane sample[39] for pulse gradient stimulated spin echo experiments, however; the same procedure under similar experimental conditions was used to measure the fluoride self-diffusion in the membrane as described earlier.[39] Water self-diffusion measurements for the $Cl^-$ form of the membrane were performed similarly using a $^1H$ coil. The experiments were carried out using a Bruker AVANCE III NMR spectrometer and 400 MHz ($^1H$ frequency) wide bore Magnex magnet. $^1H$ (400 MHz) and $^{19}F$ (376.02 MHz) diffusion measurements were made using a 5 mm Bruker single-axis DIFF60L Z-diffusion probe. The 90° pulse length was on the order of 5 µs. The range of gradient strength was 0–500 G/cm, which was incremented in 16 steps. The maximum value of the gradient was chosen such that the signal decays to 93% of the original value. The Bruker TopSpin software package was used to control the spectrometer and to analyze the data.

$$\left(\frac{S}{S_0}\right) = exp\left[-\gamma^2 G^2 \delta^2 \left(\Delta - \frac{\delta}{3}\right) D\right]$$

where $S_0$ is the signal amplitude, $\gamma$ is the gyromagnetic ratio, G is the gradient strength, $\delta$ is the length of gradient pulse (1 ms), D is the diffusion coefficient, and $\Delta$ is the time between pulses.

$\Delta$ is the time between pulses, which looks at the species diffusion as a function of various time scales. In the case of solution based system the diffusion is unrestricted and thus changing $\Delta$ will not have any effect on the value of diffusion coefficient. While in case of membrane systems, the increasing $\Delta$ gives decreasing diffusion coefficients, a phenomenon that characterizes restricted diffusion.

***Small angle X-ray scattering.—***SAXS was performed on beamline 12-ID-C at Advanced Photon Source in Argonne National Laboratory, Argonne, IL, USA. The energy of the X-ray beam was 12 keV with a wavelength of 1 Å. Spectra were collected using a Pilatus 2D detector. A custom built temperature and humidity control setup was used as described earlier.[40] SAXS spectra were collected at 60°C under 0% and 95% RH conditions. Membranes were well equilibrated before collecting the spectra. Particle size analysis was performed by Maximum entropy assuming a spheroid particle shape model using the IRENA version 6.64 SAXS package developed in Igor Pro at Argonne National Laboratory.[41]

## Results and Discussion

An insoluble, flexible, and thin membrane was formed after melt pressing at 240°C and 6000 psig. $OH^-$ back titration was used to measure IEC of both the membranes as reported in the synthesis paper.[34] For AEM-3.2, the IEC decreased after melt pressing to 3.2 $mmol.g^{-1}$, from a starting theoretical IEC of 3.8 $mmol.g^{-1}$ (ca. 16% decrease), however, for AEM-2.9 the IEC decreased only to 2.9 $mmol.g^{-1}$ from 3.3 $mmol.g^{-1}$ (ca. 12% decrease). Decrease in IEC of the membranes after melt pressing is caused by cross-linking during melt pressing followed by an incomplete quaternization with the trimethyl amine. The degree of crosslinking in the membrane seems to be proportional to the IEC of the starting polymer.

The very high $OH^-$ conductivity and stability of AEM-3.2 is illustrated in Figure 2, where a $\sigma$ = 120 mS $cm^{-1}$ at 60°C and 95%RH, is maintained for 6 days. Stable $OH^-$ conductivity >50 mS $cm^{-1}$ is indicated for practical applications.[1]

The stability is explained by the synthesis method,[34] using a diblock copolymer and a method, which was chosen deliberately to avoid bromination of the PPO block, as we have observed difficulties in measuring the $OH^-$ conductivity in AEMs ion exchanged to $OH^-$ from $Br^-$. This has been confirmed by Arges et al. recently, who observed that the membrane becomes chemically and mechanically unstable in the presence of residual bromide in the membrane.[42] This is important when our current method of hydroxide exchange needs the material to be stable to $OH^-$ for at least two weeks, one week in $OH^-$ for complete exchange and washing, and one further week to obtain steady state data (Figure 2). Reasoning for this increased stability

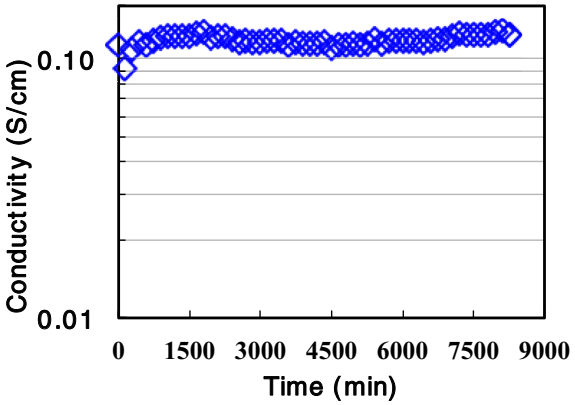


**Figure 2.** The $OH^-$ conductivity (AEM-3.2) measured at 60°C and 95%RH at under UHP $N_2$ environment.

can be attributed to absence of strong electron withdrawing groups on the aromatic backbone along with high glass transition temperature, high mechanical strength and hydrolytic stability of the PPO polymer backbone.[13] The melt pressing technique used for making the membranes promotes crosslinking and thus prevents excessive swelling under hydrated conditions of operation.

Conductivity data for both membranes as a function of temperature at 95% RH is shown as Arrhenius plots in Figure 3. For $OH^-$ the ionic conductivity was from 138 to 98 mS $cm^{-1}$ and from 106 to 63 mS $cm^{-1}$ for AEM-3.2 and AEM-2.9 at 60 and 30°C and 95%RH (Figure 3), respectively. The conductivity values for all the anions in the lower IEC film, AEM-2.9 (Figure 3, right) are lower as expected. Several research publications have reported high $OH^-$ conductivity in AEMs in a liquid water environment,[43–45] but here we report an AEM with high $OH^-$ conductivity under vapor-humidified conditions with complete exclusion of $CO_2$. Table III shows the comparison of the $OH^-$ conductivity values under complete exclusion of $CO_2$, from the literature.

The $OH^-$ conductivity shows a linear Arrhenius behavior with an $E_a$ of 9.6 and 13.5 kJ $mol^{-1}$ indicative of facile conduction with fully dissociated ion pairs (Table I). This is comparable to that reported for protons in fully humidified Nafion,[46] where the high proton conductivity is facilitated by a combination of vehicular motion and Grotthuss hopping. A recently published computational study using multiscale reactive molecular dynamic model on hydroxide transport by Chen et al. suggests that PVBTMA moieties are arranged very close together

**Table I. Arrhenius activation energy ($E_a$) of anions and water.**

| | Membrane | |
|---|---|---|
| Species | AEM-3.2 | AEM-2.9 |
| $H_2O$ | $24.9 \pm 1.2$[n] | $20.2 \pm 1.4$[n] |
| $OH^-$ | $9.6 \pm 1.0$[c] | $13.5 \pm 1.0$[c] |
| $F^-$ | - | $20.5 \pm 0.4$[n] |

[c]calculated from ionic conductivity.
[n]calculated from self-diffusion coefficient measured using PGSE-NMR.

because of the absence of long spacer chains (only 2 C atoms). The first hydration shells of each quaternary ammonium cation overlaps with each other which facilitates hydroxide transport by combination of vehicular and Grotthuss mechanisms.[22] Thus we suspect that the low activation energy observed for the AEMs in this study is a result of combination of both vehicular transport as well as Grotthuss hoping mechanism.

When the membrane in $OH^-$ form is exposed to air, $OH^-$ reacts with $CO_2$ and forms a mixture of $HCO_3^-/CO_3^{2-}$ and residual $OH^-$.[30,32,47] These bigger anions have lower ionic mobility, incomplete dissociation,[48] as shown by the deviation from linearity in the Arrhenius plot, and hence overall lower ionic conductivity. For the air exposed $OH^-$ form of AEM-3.2, the ionic conductivity was lower than 50 mS.$cm^{-1}$ at temperatures lower than 50°C at 95%RH. For AEM-3.2 even the $Cl^-$ and $HCO_3^-$ conductivities reach 87 and 97 mS.$cm^{-1}$ at 90°C and 95%RH (Figure 3). In our previous work, the ETFE-*g*-PVBTMA AEM has shown reduced ionic conductivity, which approaches the conductivity of the $HCO_3^-$ form. This indicated the formation of $HCO_3^-$ over time when $OH^-$ is exposed to air. Yan et al. have used a ratio of 3.8 to calculate the $OH^-$ conductivity from the $HCO_3^-$ form of the membrane.[33] Our results show that this ratio can only be used when the $HCO_3^-$ anion is fully dissociated and that it cannot hold when the $HCO_3^-$ ions motion is linked to the polymer through incomplete dissociation. Also for the air exposed $OH^-$ film the ratio of $OH^-$ to $HCO_3^-$ is not constant as we sweep temperature and humidity. The ratio was 5.5 at 30°C and reduced to 2.7 at 60°C.

The drop in conductivity of AEM-3.2 when exposed to air, and curvature of the data on an Arrhenius plot indicates Vogel–Tammann–Fulcher (VTF) behavior as the ions are no longer fully dissociated and move with the dynamics of the host polymer.[45,49] Marino et al. have observed similar weak dissociation behavior at lower hydration levels in AEMs which are exchanged with halides or $HCO_3^-$ even though the quaternary ammonium salts dissociate

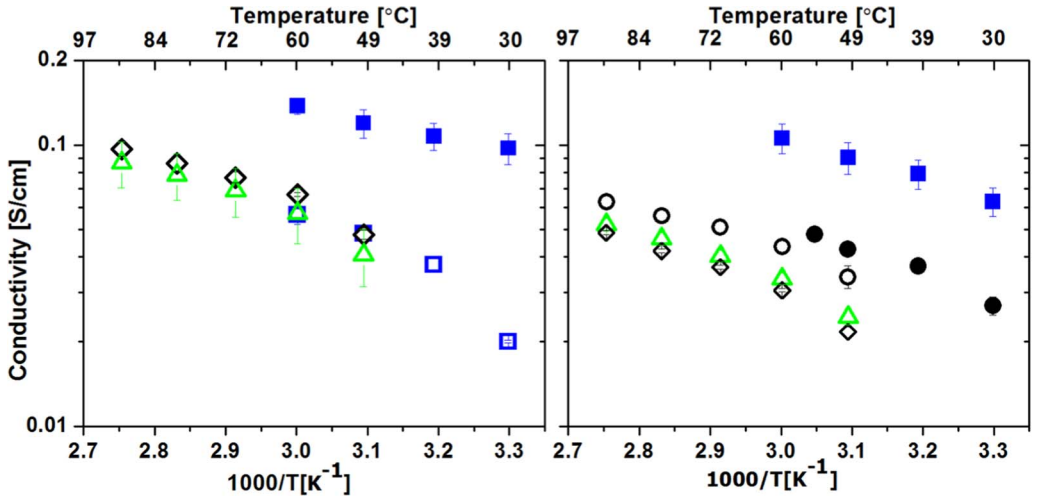


**Figure 3.** Conductivity for different ionic forms on an Arrhenius plot, $OH^-$ (■), air exposed $OH^-$ (□), $HCO_3^-$ (◊), $Cl^-$ (△), and $F^-$ measured (◯) and calculated from PGSE diffusion NMR (●) for AEM-3.2 (left) and AEM-2.9 (right) at 95%RH as a function of temperature.

**Table II. VTF fitting parameters for AEM-3.2 and AEM-2.9.**

| | A | | $E_i$ (kJ/mol) | | $T_0$ (K) | |
|---|---|---|---|---|---|---|
| Counter - anions | AEM-3.2 | AEM-2.9 | AEM-3.2 | AEM-2.9 | AEM-3.2 | AEM-2.9 |
| $HCO_3^-$ | 3.6 | 2.6 | 0.43 | 0.77 | 286 | 274 |
| $Cl^-$ | 3.2 | 2.5 | 0.40 | 0.66 | 290 | 277 |
| $F^-$ | - | 2.6 | - | 0.59 | - | 274 |

completely in aqueous solution.[48] These undissociated ion pairs and presence of water in the channels makes the entire system somewhat more complex. When the film is fully exchanged to the $HCO_3^-$ form similar ionic conductivity and behavior is observed. $Cl^-$ also shows similar VTF behavior and interestingly has approximately the same conductivity values as $HCO_3^-$ ions (ca. 85–90 mS $cm^{-1}$) at 95% RH and 90°C in AEM-3.2. The conductivity data was fitted to VTF equation 1 as follows,

$$\sigma_i = AT^{-1/2}e^{-E_i/R(T-T_o)}$$

where A is a constant proportional to the number of charge carriers, R is the gas constant, $E_i$ is the pseudo-activation energy, and $T_0$ is the thermodynamic ideal glass transition temperature at which the configurational entropy becomes zero or the "free volume" disappears (Table II).[45] Values of A were in the range of 3.2–3.6 for AEM-3.2 and 2.5–2.6 for AEM-2.9. Values of A increase with the IEC as expected. The $T_0$ value ranges between 1 and 27°C for both membranes.

The parameter A is proportional to number of free ions/charge carriers in the polymer electrolyte and was found to increase with increasing IEC for both the membranes. Activation energy obtained from VTF theory incorporates entropy in it and thus it cannot be compared to activation energy obtained by Arrhenius equation. Usually a thermal transition exists for polymer electrolytes at $T_0 + 40$°C. Many of the previously studied materials had a transition temperature, which was below freezing.[50,51] In our case the calculated transition temperature falls in the operating region of a fuel cell, above such thermal transition temperature, segmental motion of the chains facilitates ion transport.

The $F^-$ conductivity was also measured for AEM-2.9 (Figure 3). It can be seen that $F^-$ conductivity is higher than that for $Cl^-$ as $F^-$ is smaller than $Cl^-$, and both show the non-dissociated VTF behavior discussed above.

Figure 4 shows the $OH^-$ conductivity as a function of RH for AEM-3.2 and for the same film exposed to air. The $OH^-$ conductivity of the membrane decreased when the RH was decreased from 95% to 80% RH by 138 to 91 mS $cm^{-1}$ and is still at a practical value of 44 mS $cm^{-1}$ at a relatively low 60% RH. The conductivity of the air-exposed membrane goes down more significantly with the lowering of the RH and the ratio of the conductivity of the $OH^-$ and air exposed $OH^-$ film increases from ca. 2.6 to 17 mS $cm^{-1}$ with decreasing humidity.

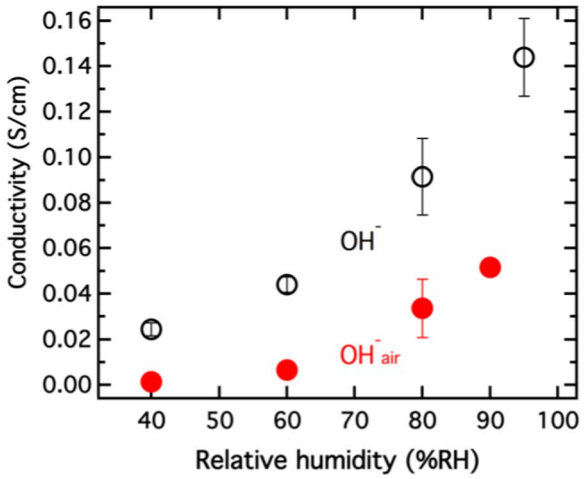


**Figure 4.** $OH^-$ (○) vs air exposed $OH^-$ (●) conductivity for AEM-3.2 at 60°C as a function of relative humidity.

The water uptake of the $Cl^-$ form of the membranes at 95%RH and 60°C shows λ values of 8.7 and 10.5 for AEM-3.2 and AEM-2.9; respectively (Figures 5a and 5b). At 30°C the λ value for the AEM-3.2 was 6. The more crosslinked AEM-3.2 seems to swell less under RH than AEM-2.9, but this trend is reversed when the films are immersed in liquid water. While it was not possible for us to measure λ from water vapor for the reactive anion, we did compare $Cl^-$, $HCO_3^-$, and $OH^-$ from liquid water (SI Figure S3). The magnitude of water uptake increases with IEC and in the series $Cl^- < HCO_3^- < OH^-$ making it reasonable to assume that the $OH^-$ forms of AEM-3.2 and AEM-2.9 will have ca. 25% more water per anion, λ than $Cl^-$ (SI Figure S3). A decent $OH^-$ conductivity even at 60% RH and 60°C was observed for $OH^-$ form of the membrane due to better water retention properties at low RH (λ of 4–6 under 60%RH at 60°C). It has been shown that just 4 water molecules are enough to completely solvate the $OH^-$ ion[20] and so the $OH^-$ remains fully dissociated with fast transport even when the film is not fully saturated with water. Dimensional

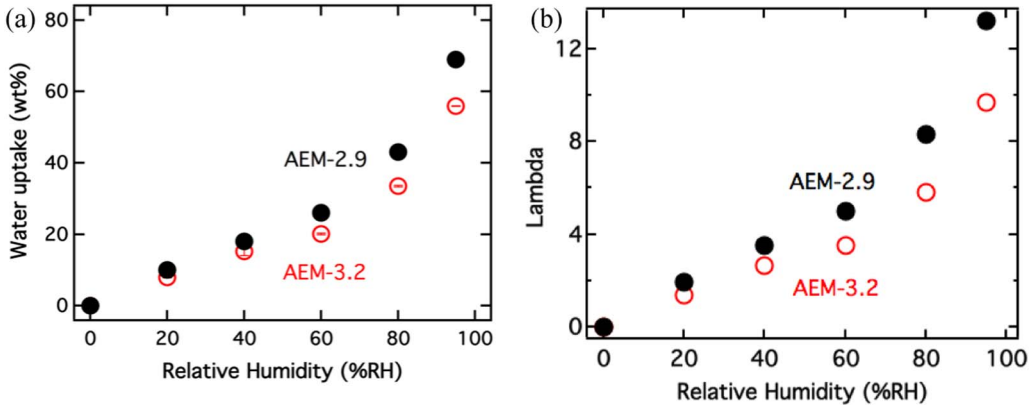


**Figure 5.** a) Vapor % water uptake by the AEM-3.2 and AEM-2.9 at 60°C b) Lambda by the AEM-3.2 and AEM-2.9 at 60°C calculated from % vapor water uptake.

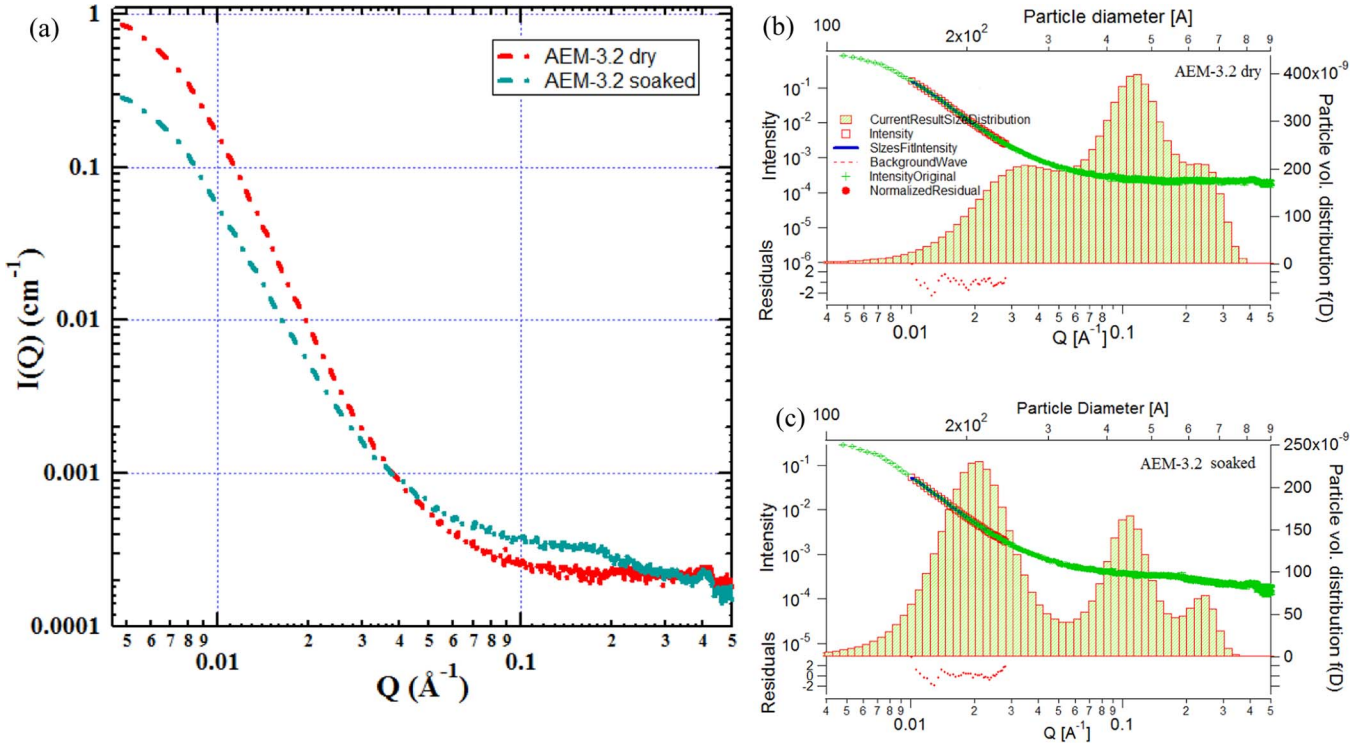


**Figure 6.** (a) Small Angle X-ray Scattering (SAXS) pattern of dry and soaked AEM-3.2 in bromide form at 60°C, Particle size analysis for domain sizes in AEM-3.2 for both dry (b), and soaked (c) samples, showed a growing peak at 200 Å when membrane was hydrated.

**Table III. Comparison of $OH^-$ conductivity to water uptake of our membranes to literature.**

| Membranes | IEC (mmol/g) | $OH^-$ Conductivity (mS/cm) | Lambda |
|---|---|---|---|
| Non crosslinked FAA-3 (FuMaTech GmbH) | 2.1 | ~65 (25°C, water) | 45 (25°C, $Cl^-$ [48]) |
| ETFE-*g*-PVBTMA | 1.8 | 112 ± 20 (60°C, 95% RH) | 3.7 (30°C, $Cl^-$ [32]) |
| AEM-3.2 | 3.2 | 138 (60°C, 95% RH) | 8.7 (60°C, $Cl^-$) (this work) |
| AEM-2.9 | 2.9 | 106 (60°C, 95% RH) | 10.5 (60°C, $Cl^-$) (this work) |

change measurement on AEM-3.2 indicated through-plane, and in-plane swelling by ca. 65 and 50%; respectively (SI Figure S4).

We probed the uptake of the water in the microstructure of AEM-3.2 by SAXS (Figure 6). The membranes were exchanged into the bromide form to enhance scattering. Figure 6 shows the SAXS pattern of dry and soaked AEM-3.2 at 60°C. A broad peak grows in the range of 0.06–0.2 Å$^{-1}$, corresponding to a d-spacing of 3.5 nm at its maximum. In PEM literature, these peaks are usually assigned to an ionomer peak.[52] Here, we assign it to water directly associated with the ion pairs. Additional water appears to go into other domains in the membrane.[32] The Porod slope in the region of 0.01–0.028 Å$^{-1}$ when dry is 4.2 and decreased to 3.3 upon hydration, attributed to the spheroidal particles becoming elongated. The particle size distribution analysis in this region shows ca. 44 nm size domains when the membrane is dry. Upon hydration in addition to these ca. 44 nm hydrophobic domains, and the hydrated ion-pair clusters, ca. 3.5 nm, there is the development of additional water rich ca. 20 nm and ca. 62 nm domains (Figure 6c). Further proof that the ca. 44 nm domains are the hydrophobic domains comes from a comparison of these SAXS analysis to the TEM images previously published work[34] which shows the presence of spherical 40–45 nm clusters in the same polymer (Figure 7).

The microstructure of the polymer in cartoon form is shown in Figure 7. The PPO block (red color) formed domain size of 44 nm calculated from SAXS particle size analysis at both dry and wet conditions. The hydrophilic block with quaternary trimethyl ammonium (light blue) polymer with a positive charge at the end is bonded to

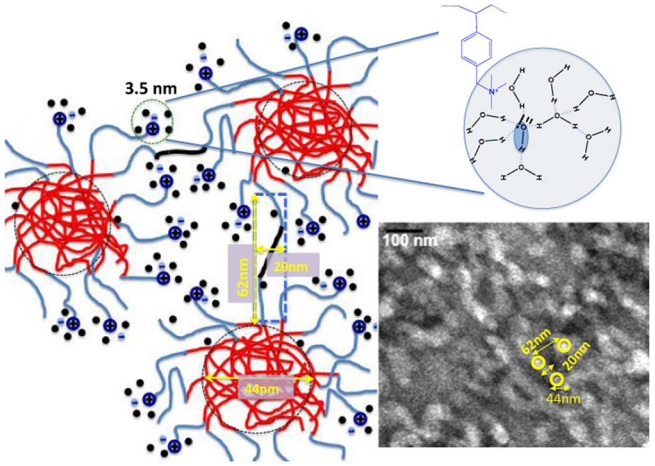


**Figure 7.** Schematic of polymer microstructure at saturated hydration conditions. PPO (red), PVBCTMA (light blue with positive charge), PVBC (light blue), water (black solid circle), hydroxide (blue solid with negative charge). A black polymer segment joining two light blue polymer microstructure indicates the presence of crosslinking in the membrane. A TEM image of AEM-3.2 (PPO-b-PVBTMA12 in literature),[34] put together to show the size domains in the membrane calculated from SAXS analysis, blue bubble highlights water co-ordination with $OH^-$ for Grotthuss hopping mechanism. TEM micrograph reprinted with permission from *Macromolecules*, **48**, 4471–4480 (2015) © 2015, American Chemical Society.

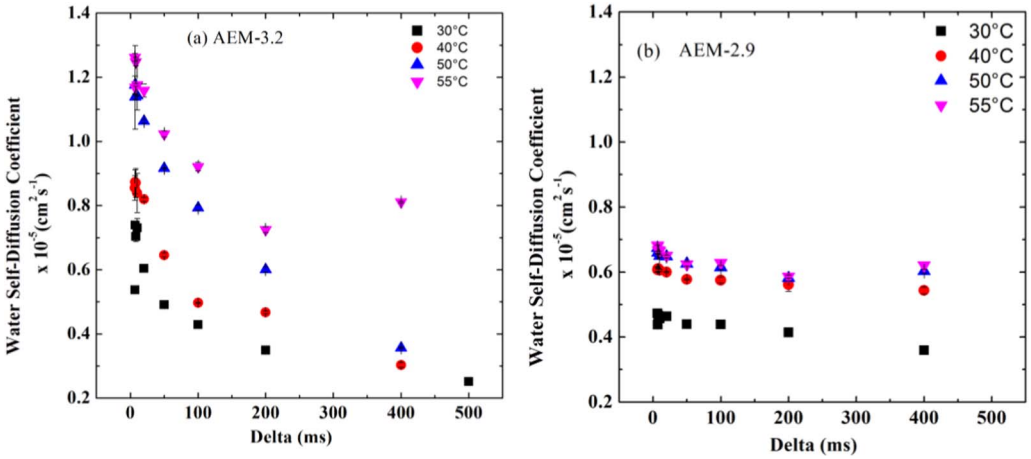


**Figure 8.** Water self-diffusion coefficient of (a) AEM-3.2 and (b) AEM-2.9 measured using PGSE-NMR under saturated humidity as a function of temperature.

$OH^-$ (blue negative charge) and at least four water molecules (black). Few polymer strands without positive charge represents a possibility of an incomplete quaternization, and a black connection between unquaternized strands indicates the thermal crosslinked bridges formed during melt pressing. A red dotted circle represents a cluster of ions that forms a peak of size of 3.5 nm in SAXS. At hydrated conditions, as indicated by both TEM and SAXS, these polymer domains separate themselves apart by 62 nm with a 20 nm wide domain. These values correlated in AEM-3.2 where both TEM and SAXS measurement were performed at same $Br^-$ anion form. To emphasize the transport Grotthuss mechanism of $OH^-$ that contributed for high $OH^-$ conductivity, a simple schematic (blue bubble) shows the $OH^-$ co-ordination with water molecules based on theoretical work.[22,53]

We studied both the water and the $F^-$ self-diffusion by PGSE NMR. For water a one component fit to the Gaussian decay of the data could not represent the data. A two-component model gave two diffusion coefficients, one for water associated with the ion pairs (3.5 nm domains), and another for the other water domains in the membrane (20 nm domains). Figure 8 shows the ion-pair cluster water self-diffusion as a function of temperature and diffusion time for AEM-3.2, and AEM-2.9. Interestingly, the $E_a$ for water self-diffusion of these two films is 24.9 and 20.2 kJ $mol^{-1}$, respectively, twice that for $OH^-$ conductivity (Table I), further evidence that $OH^-$ conductivity may have a Grotthuss component, in addition to vehicular transport. The water self-diffusion coefficients reported here are in agreement with self-diffusion coefficients reported for associated water in Polyphenylene and (phenylene alkylene) based AEMs studied by Alam et al.[54] further proving that the diffusion seen here is from the water associated with the ion pair cluster. The $F^-$ ion which is ca. the same size as $OH^-$ can be used as a surrogate ion for $OH^-$ that can only move via a vehicular mechanism.[32] An attempt was made to measure $F^-$ self-diffusion in AEM-3.2, but the spin lattice relaxation, $T_1$, for AEM-3.2 was too small (25 ms) to enable the PGSE NMR measurement. This was not the case for AEM-2.9, $T_1 > 300$ ms and so this membrane was used for the $F^-$ PGSE NMR experiments, Figure 9. As the $F^-$ self-diffusion data showed a linear trend on an Arrhenius plot, with $E_a = 20.5$ kJ $mol^{-1}$ we were able to use the Nernst-Einstein equation to calculate the conductivities which are plotted on Figure 3 (●) and show good agreement with the measured values of the $F^-$ conductivity. The $E_a$ of 20.5 kJ $mol^{-1}$ for $F^-$ self-diffusion is in excellent agreement with the $H_2O$ value of 20.2 kJ $mol^{-1}$. Clearly vehicular transport of $F^-$ has a higher activation than the Grotthuss modulated $OH^-$ transport, $E_a =$ 13.5 kJ $mol^{-1}$ for AEM-2.9.

To further correlate this data with structure we analyzed the self-diffusion coefficients as a function of diffusion time by the Mitra equation (Table S1-S3).[55] Using the fluoride self-diffusion coefficients obtained from the NMR, a tortuosity of ~1.3 was observed for the AEM-2.9 which was slightly higher than the water diffusion measurements for AEM-2.9 which resulted in a tortuosity of 1.2. A tortuosity of 1.8 was obtained for AEM-3.2 using water self-diffusion measurements, which can be attributed to the more crosslinked nature of the AEM-3.2.

## Conclusions

In conclusion we have shown that a cross-linked PPO-*b*-PVBTMA with high IEC is not only highly stable at 60°C and 95%RH for 2 weeks, but also highly conductive to $OH^-$. Conductivity, water uptake and ion transport measurements we performed at drier conditions are very important for practical applications. The $OH^-$ conductivity measurements were performed at 95%RH totally excluding $CO_2$ environment. The $OH^-$ ions are fully dissociated under saturated humidified conditions and always show Arrhenius behavior under the conditions studied. The high conductivity of $OH^-$ can be explained by a combination of both Grotthuss hopping and vehicular transport. $OH^-$ ions are fully dissociated under fully humidified conditions in the AEM and thus follow Arrhenius behavior, but for bigger anions or a combination of ions ion dissociation is somehow limited by

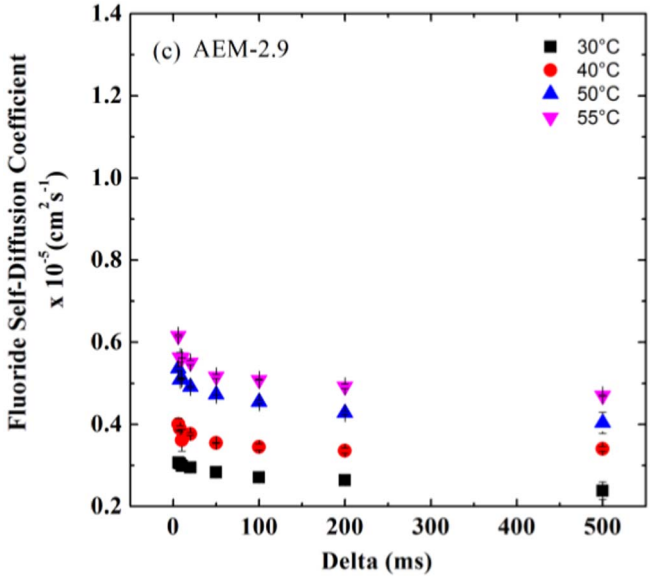


**Figure 9.** Fluoride self-diffusion measurements for AEM-2.9 measured using PGSE NMR.

dissolution enthalpies of ions in the presence of slightly lower amount of water.[48] Lower dissociation of halide or $HCO_3^-$ ions and presence of water in the hydrophilic channels make the ion transport complex and cannot be explained by only Arrhenius behavior. Thus we infer that the ions are moving by the dynamics of the host polymer (VTF theory) modulated by water. Even so the $Cl^-$ and $HCO_3^-$ conductivities are very high at 90°C and 95%RH. The water in the fully humidified films is shown to be in several different domains, the smaller of which is associated with the cation anion pair as shown by SAXS. More studies are required to understand the distribution of water in other domains. With hydration, the core PPO size domain (44 nm) was not changed, but other two domains (20 nm and 62 nm) were observed in the SAXS, which was confirmed from TEM micrographs for AEM-3.2. High conductivity, good chemical stability, faster ion diffusion, and good mechanical strength are some of the outstanding properties, which are of interest for consideration of the use of the polymers in practical devices.

## Acknowledgment

The authors thank the Army Research Office for support of this research under the MURI program, grant W911NF-11-1-0462, and The Colorado School of Mines NMR facility funded by National Science Foundation under an MRI grant CHE-0923537. This research used resources of the Advanced Photon Source, a U.S. Department of Energy (DOE) Office of Science User Facility operated for the DOE Office of Science by Argonne National Laboratory under Contract No. DE-AC02-06CH11357.

## References

1. J. R. Varcoe, P. Atanassov, D. R. Dekel, A. M. Herring, M. A. Hickner, P. A. Kohl, A. R. Kucernak, W. E. Mustain, K. Nijmeijer, K. Scott, T. Xu, and L. Zhuang, *Energy & Environmental Science.*, **7**, 3135 (2014).
2. J. S. Spendelow and A. Wieckowski, *Physical Chemistry Chemical Physics.*, **9**, 2654 (2007).
3. G. Merle, M. Wessling, and K. Nijmeijer, *Journal of Membrane Science.*, **377**, 1 (2011).
4. M. R. Hibbs, *Journal of Polymer Science Part B: Polymer Physics.*, **51**, 1736 (2013).
5. M. A. Hickner, A. M. Herring, and E. B. Coughlin, *Journal of Polymer Science Part B: Polymer Physics.*, **51**, 1727 (2013).
6. F. Zhang, H. Zhang, and C. Qu, *Journal of Materials Chemistry.*, **21**, 12744 (2011).
7. A. D. Mohanty, Y. B. Lee, L. Zhu, M. A. Hickner, and C. Bae, *Macromolecules.*, **47**, 1973 (2014).
8. J. Yan and M. A. Hickner, *Macromolecules.*, **43**, 2349 (2010).
9. X. Lin, X. Liang, S. D. Poynton, J. R. Varcoe, A. L. Ong, J. Ran, Y. Li, Q. Li, and T. Xu, *Journal of Membrane Science.*, **443**, 193 (2013).
10. N. Li, Y. Leng, M. A. Hickner, and C. Y. Wang, *Journal of the American Chemical Society.*, **135**, 10124 (2013).
11. X. Lin, L. Wu, Y. Liu, A. L. Ong, S. D. Poynton, J. R. Varcoe, and T. Xu, *Journal of Power Sources.*, **217**, 373 (2012).
12. X. Wu, W. Chen, X. Yan, G. He, J. Wang, Y. Zhang, and X. Zhu, *Journal of Materials Chemistry A.* **2**, 12222 (2014).
13. T. Xu, D. Wu, and L. Wu, *Progress in Polymer Science.*, **33**, 894 (2008).
14. J. Ran, L. Wu, B. Wei, Y. Chen, and T. Xu, *Scientific Reports.*, **4**, 6486 (2014).
15. J. Ran, L. Wu, J. R. Varcoe, A. L. Ong, S. D. Poynton, and T. Xu, *Journal of Membrane Science.*, **415**, 242 (2012).
16. X. Lin, J. R. Varcoe, S. D. Poynton, X. Liang, A. L. Ong, J. Ran, Y. Li, and T. Xu, *Journal of Materials Chemistry A.*, **1**, 7262 (2013).
17. C. G. Arges, L. Wang, J. Parrondo, and V. Ramani, *Journal of The Electrochemical Society.*, **160**, F1258 (2013).
18. J. E. Jenkins, M. R. Hibbs, and T. M. Alam, *Acs Macro Letters.*, **1**, 910 (2012).
19. W. M. Haynes, D. R. Lide, and T. J. Bruno, *CRC Handbook of Chemistry and Physics*, CRC Press, 2012.
20. M. E. Tuckerman, D. Marx, and M. Parrinello, *Nature.*, **417**, 925 (2002).
21. K. N. Grew and W. K. S. Chiu, *Journal of the Electrochemical Society.*, **157**, B327 (2010).
22. C. Chen, Y.-L. S. Tse, G. E. Lindberg, C. Knight, and G. A. Voth, *Journal of the American Chemical Society.*, **138**, 991 (2016).
23. V. Di Noto, G. A. Giffin, K. Vezzu, G. Nawn, F. Bertasi, T.-H. Tsai, A. M. Maes, S. Seifert, E. B. Coughlin, and A. M. Herring, *Physical Chemistry Chemical Physics.*, **17**, 31125 (2015).
24. N. Li, Q. Zhang, C. Wang, Y. M. Lee, and M. D. Guiver, *Macromolecules.*, **45**, 2411 (2012).
25. Q. Li, L. Liu, Q. Miao, B. Jin, and R. Bai, *Chemical Communications.*, **50**, 2791 (2014).
26. N. T. Rebeck, Y. Li, and D. M. Knauss, *Journal of Polymer Science Part B: Polymer Physics.*, **51**, 1770 (2013).
27. Q. Li, L. Liu, Q. Miao, B. Jin, and R. Bai, *Polymer Chemistry.*, **5**, 2208 (2014).
28. J. Ran, L. Wu, B. Wei, Y. Chen, and T. Xu, *Sci. Rep.*, **4**, 6486 (2014).
29. H.-S. Dang and P. Jannasch, *Macromolecules.*, **48**, 5742 (2015).
30. Y. Hiroyuki and F. Kenji, *ECS Transactions.*, **16**, 257 (2008).
31. O. D. Thomas, K. J. W. Y. Soo, T. J. Peckham, M. P. Kulkarni, and S. Holdcroft, *Journal of the American Chemical Society.*, **134**, 10753 (2012).
32. T. P. Pandey, A. M. Maes, H. N. Sarode, B. D. Peters, S. Lavina, K. Vezzu, Y. Yang, S. D. Poynton, J. R. Varcoe, S. Seifert, M. W. Liberatore, V. Di Noto, and A. M. Herring, *Physical Chemistry Chemical Physics.*, **17**, 4367 (2015).
33. J. Yan and M. A. Hickner, *Macromolecules.*, **43**, 2349 (2010).
34. Y. Yang and D. M. Knauss, *Macromolecules.*, **48**, 4471 (2015).
35. A. K. Mukherjee and A. Gupta, *Journal of Macromolecular Science, Part C.* **20**, 309 (1981).
36. A. M. Maes, T. P. Pandey, M. A. Vandiver, L. K. Lundquist, Y. Yang, J. L. Horan, A. Krosovsky, M. W. Liberatore, S. Seifert, and A. M. Herring, *Electrochimica Acta.*, **110**, 260 (2013).
37. T. P. Pandey, A. M. Maes, H. N. Sarode, B. D. Peters, S. Lavina, K. Vezzu, Y. Yang, S. D. Poynton, J. R. Varcoe, S. Seifert, M. W. Liberatore, V. Di Noto, and A. M. Herring, *Physical Chemistry Chemical Physics.*, **17**, 4367 (2015).
38. K. J. Noonan, K. M. Hugar, H. A. T. Kostalik, E. B. Lobkovsky, H. D. Abruna, and G. W. Coates, *J Am Chem Soc.*, **134**, 18161 (2012).
39. Y.-L. S. Tse, H. N. Sarode, G. E. Lindberg, T. A. Witten, Y. Yang, A. M. Herring, and G. A. Voth, *The Journal of Physical Chemistry C.* **118**, 845 (2014).
40. Y. Liu, J. L. Horan, G. J. Schlichting, B. R. Caire, M. W. Liberatore, S. J. Hamrock, G. M. Haugen, M. A. Yandrasits, S. Seifert, and A. M. Herring, *Macromolecules.*, **45**, 7495 (2012).
41. J. Ilavsky and P. R. Jemian, *J Appl Crystallogr.*, 347 (2009).
42. C. G. Arges, L. Wang, M.-S. Jung, and V. Ramani, *Journal of The Electrochemical Society.*, **162**, F686 (2015).
43. N. J. Robertson, H. A. T. Kostalik, T. J. Clark, P. F. Mutolo, H. D. Abruna, and G. W. Coates, *J Am Chem Soc.*, **132**, 3400 (2010).
44. Q. Li, L. Liu, Q. Q. Miao, B. K. Jin, and R. K. Bai, *Polymer Chemistry.*, **5**, 2208 (2014).
45. G. A. Giffin, G. M. Haugen, S. J. Hamrock, and V. Di Noto, *Journal of the American Chemical Society.*, **135**, 822 (2013).
46. M. Cappadonia, J. W. Erning, S. M. S. Niaki, and U. Stimming, *Solid State Ionics.*, **77**, 65 (1995).
47. M. G. Marino and K. D. Kreuer, *ChemSusChem.*, **8**, 513 (2015).
48. M. G. Marino, J. P. Melchior, A. Wohlfarth, and K. D. Kreuer, *Journal of Membrane Science.*, **464**, 61 (2014).
49. V. Di Noto, D. Longo, and V. Münchow, *The Journal of Physical Chemistry B.* **103**, 2636 (1999).
50. F. Croce, M. L. Focarete, J. Hassoun, I. Meschini, and B. Scrosati, *Energy & Environmental Science.*, **4**, 921 (2011).
51. V. Di Noto, M. Vittadello, S. Lavina, M. Fauri, and S. Biscazzo, *Journal of Physical Chemistry B.* **105**, 4584 (2001).
52. H. G. Haubold, T. Vad, H. Jungbluth, and P. Hiller, *Electrochimica Acta.*, **46**, 1559 (2001).
53. M. E. Tuckerman, D. Marx and M. Parrincelo. *Nature.*, **417**, 925 (2002).
54. T. M. Alam and M. R. Hibbs, *Macromolecules.*, **47**, 1073 (2014).
55. P. P. Mitra, P. N. Sen, and L. M. Schwartz, *Physical Review B.* **47**, 8565 (1993).